11

High Gain Solid-State Amplifiers for Picosecond Pulses

Antonio Agnesi and Federico Pirzio
Laboratorio Sorgenti Laser
Dipartimento di Elettronica dell'Università di Pavia
Via Ferrata 1 - 27100 Pavia
Italy

1. Introduction

Picosecond solid-state lasers are attractive for many industrial and scientific applications, such as precision material processing (Dausinger et al., 2003; Breitling et al., 2004), nonlinear optics (McCarthy & Hanna 1993; Ruffling et al., 2001; Sun et al., 2007) and laser spectroscopy (Mani et al., 2001). In contrast with traditional laser processing performed with 10-100 ns multi-kHz sources, picosecond laser-matter interaction is basically non-thermal, relying on multi-photon ionisation and photo-ablation processes that allow cleaner and much higher spatial definition in laser marking, drilling and cutting. Femtosecond pulses would perform even better in principle, but at the expense of a significant increase in complexity of the laser system that most often is unwelcome in industrial environments.

Furthermore, the multi-kW peak-power levels allowed by cw mode-locked picosecond lasers with average power of at least few watts are already sufficient to produce efficient frequency conversion by harmonic, sum- or difference-mixing and parametric generation.

Semiconductor saturable absorber mirrors (SESAMs) are widely employed for the passive mode-locking of picosecond solid-state lasers (Keller, 2003). SESAMs are very effective and highly reliable when used in low-power oscillators; however, when employed in high-power oscillators, they require a special design as their thermal management becomes a very important issue (Burns et al., 2000; Neuhaus et al., 2008). Indeed, the intense intracavity radiation of this particular operating regime may induce significant optical and thermo-mechanic stress effects, leading to rapid degradation of their performance.

An alternative (and not new) approach to powerful cw picosecond sources is to use a master-oscillator power-amplifier (MOPA) system, in which a seed from a low-power, robust picosecond laser is amplified to the required average power levels through extra-cavity diode-pumped amplifiers.

Some recent results have pointed out the great potential of this approach (Snell et al., 2000; Agnesi et al., 2006a; Nawata et al., 2006; Farrell & Damzen, 2007; McDonagh et al., 2007). To our knowledge, the most powerful cw picosecond source reported to date was a Nd:YVO_4 MOPA system longitudinally-pumped with 216 W at 888 nm, where a 60-W cw picosecond mode-locked laser was amplified to 111 W, with 53% amplifier extraction efficiency (McDonagh et al., 2007). Though the master oscillator of this example could be well

Source: Advances in Solid-State Lasers: Development and Applications, Book edited by: Mikhail Grishin,
ISBN 978-953-7619-80-0, pp. 630, February 2010, INTECH, Croatia, downloaded from SCIYO.COM

classified as "high-power", the effectiveness and the convenience of the power amplification to reach very high power levels is clear.

It is also worth noticing that fibre laser technology is rapidly approaching maturity also in the field of high-power ultrafast laser applications (Fermann & Hartl, 2009), though reliable large-area, photonic fibres sustaining picosecond pulses with energy >1 μJ are still subject of extensive research. Most likely, this will take some time before full commercial exploitation. Indeed, all-fibre amplification of femtosecond pulses, stretched to nanosecond or sub-nanosecond time duration, is definitely easier than direct amplification of pulses only few picosecond long. However, robust picosecond master oscillators, passively mode-locked by SESAMs (Okhotnikov et al., 2003) or other techniques (Porta et al., 1998), can be successfully realised with readily available fibre laser components. These considerations suggest an attractive approach to picosecond MOPAs consisting in a compact rugged picosecond fibre oscillator and a powerful diode-pumped solid-state amplifier with mode size properly scaled in order to avoid damage.

Grazing-incidence side-pumped Nd:YVO_4 slabs allow efficient power extraction owing to the very high single-pass gain achievable in such configuration (Bernard & Alcock, 1993; Damzen et al., 2001). This article reviews picosecond MOPA systems employing this particular amplification technique. Simple numerical models are presented and applied to the design of MOPAs, as well as for the interpretation of their performance and limitations.

A four-pass amplification setup including a photo-refractive phase-conjugating mirror was first reported to yield 12.8 W, nearly diffraction-limited, 8.7-ps pulses (Ojima et al., 2005) starting from a 100-MHz, 290-mW commercial cw mode-locked Nd:YVO_4 master oscillator. An improved and more powerful setup also employing phase-conjugating mirror delivered up to 25 W (Nawata et al., 2006).

A simpler setup with either a single- or double-pass slab yielded as much as 8.4 W with 7.5-ps pulses at 150 MHz (30% amplifier extraction efficiency from 28-W pump power), using a 50-mW seed oscillator (Agnesi et al., 2006a).

Other applications require instead intense picosecond pulses from compact diode-pumped solid-state laser systems at lower repetition rates ($\lesssim$1 MHz). Usually, intra- or extra-cavity pulse-picking from a diode-pumped low-power picosecond oscillator at ~ 100-MHz repetition rate is used to seed a regenerative amplifier. By this means, the pulse energy is increased from nanojoules to within a range from few microjoules to few millijoules, depending on the operating frequency (Siebold et al., 2004; Kleinbauer et al., 2005; Killi et al., 2005).

For this aim, too, grazing-incidence bounce amplifiers provide an interesting alternative, since their gain of ≈ 30 dB/pass allows efficient energy extraction in just two or three passes, thus avoiding the higher complexity of the former schemes and requiring only a versatile, extra-cavity acousto-optic pulse-picker. This needs to be appropriately synchronised to the mode-locked train, as well as to the amplifier pump pulse (if the amplifier is not cw-pumped).

In the first demonstration of such an amplifying configuration, the high-frequency picosecond seeder output was sampled synchronously, and the selected pulse (with energy < 1 nJ) was injected into a two-stage amplifier, yielding an output energy up to 10 μJ at 100 Hz (Agnesi et al., 2006b). A remarkable 1-MHz high repetition frequency and pulse energy up to 76 μJ were later reported by Nawata *et al.*, (Nawata et al., 2007) who employed a more complex cw-pumped phase-conjugation setup with a double-pass grazing-incidence slab. Repetition frequency as high as 4 MHz was also reported for an extra-cavity multi-pass

Nd:YVO_4 amplifier (Gerhard et al., 2008), yielding 80 μJ at low frequency and 1.8 μJ at 4 MHz. Effective material processing results were demonstrated with such a laser system.
However, the highest pulse energy was achieved with a refined qcw-pumped single-pass two-slabs amplifier design (Agnesi et al., 2008a), yielding as much as 210 μJ, up to 1 kHz repetition rate, and 11-ps time duration pulses.
Highly efficient harmonic conversion to 532 nm and 266 nm was readily observed, owing to the ≈ 20-MW peak power of the amplified picosecond pulses.
Travelling-wave parametric generation spanning the ranges 770-1020 nm (signal), 1110-1720 nm (idler) was also demonstrated (Agnesi et al., 2006b).
Particular applications such as photocatode injection (Will et al., 2005), low-threshold parametric generation (Agnesi et al., 1993; Butterworth et al., 1996) and implementation of pulse-format and wavelength typical of free-electron-lasers (Edwards et al., 2002) by all-solid-state laser technology require instead amplification of bunches of picosecond pulses.
Again, side-pumped high-gain bounce amplifiers can be successfully employed to increase the pulse energy of pulse trains as long as ~ 1 μs. A remarkable example of such a laser source delivering trains of ~ 2500 pulses of 12-ps time duration, 5-GHz repetition rate at 1064 nm, and train energy of 250 mJ, was reported recently (Agnesi et al., 2008b). This review is organised as follows. Section 2 gives the theoretical background for understanding and modelling grazing-incidence slab amplifiers; Sections 3-5 review some representative experimental results achieved by our research group with slab amplifiers operated in several regimes, as well as interesting frequency conversion applications; in Section 6 we finally summarise our results and trace few conclusions.

2. Numerical model

In this Section we review simple, yet effective, numerical models for grazing-incidence class of amplifiers, for several operating regimes such as cw and pulsed up to multi-kHz repetition rate. Limitations due to the finite amplifying bandwidth are discussed. These models will be applied to the interpretation of experimental results reviewed in the next Sections. More generally, their use extends to a wider class of amplifier, including, for example, cascaded systems and bounce amplifiers based on different laser materials, provided the pump absorption depth is of the order of ~ 1 mm or less, and the integrated single-pass gain reaches useful levels.

2.1 Operation in cw regime

The model is based on standard cw amplifier theory (Koechner, 2006). Let us introduce a reference system for bounce beam propagation in the active material slab shown in Fig. 1. The length and the thickness of the slab are L and W, respectively.
A particularly useful transverse local frame for the seed beam is ξ–y. Assuming small grazing angles, i.e. $\theta \ll 1$ rad, we may approximate $x(s, \xi) = \theta L/2 + \xi - s\theta$. The propagation inside the amplifier occurs with a nearly-constant beam cross section in order to optimise the overlap efficiency, therefore the gain can be calculated along the longitudinal s coordinate as in a ray-tracing approximation:

$$\frac{dI(\xi, y)}{ds} = \sigma n(x, y) I(\xi, y) \tag{1}$$

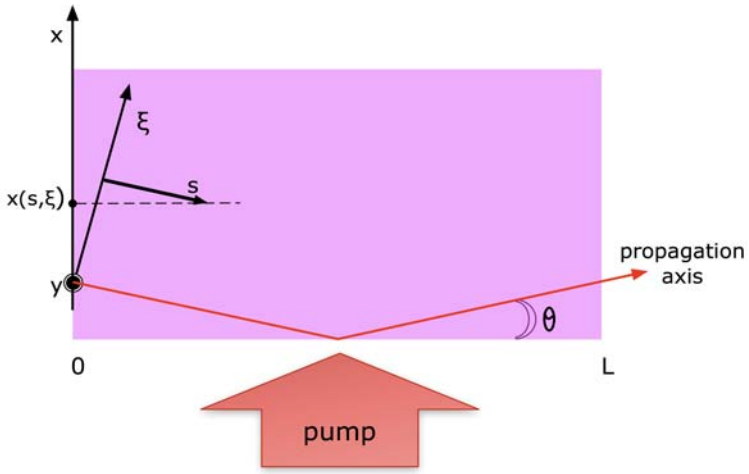

Fig. 1. Model of the slab amplifier (seen from above): the beam enters from the left side with a grazing angle θ. The beam cross section is most easily described by coordinates (ξ,y).

The saturated population inversion density is

$$n(x,y) = \frac{R_p(x,y)\tau}{1 + I(\xi,y)/I_S} \tag{2}$$

and the pump rate is given by

$$R_p(x,y) = \frac{\lambda_P}{\lambda_L}\frac{\alpha_p}{WL}\frac{P_{inc}\Theta(y)e^{-\alpha_p x}}{h\nu} \tag{3}$$

The step function Θ is defined as: $\Theta(y) = 1$ for $|y| < W/2$, $\Theta(y) = 0$ for $|y| > W/2$; σ is the stimulated emission cross section at the laser frequency $\nu = c/\lambda_L$; τ is the fluorescence time; $I_s = h\nu/(\sigma\tau)$ is the laser saturation intensity; α_P is the saturated absorption coefficient at the pump wavelength λ_P, corresponding to the incident pump intensity $I_P = P_{inc}/(WL)$ (P_{inc} is the power transmitted through the pump face and absorbed by the crystal), $\alpha_P = \alpha_{P0}/(1 + I_P/I_{SP})$ and I_{SP} is the pump absorption saturation intensity (Bermudez et al., 2002).
Inserting Eqs. (2) and (3) into Eq. (1) and integrating, one obtains

$$\ln\left[\frac{I_o(\xi,y)}{I_i(\xi,y)}\right] + \frac{I_o(\xi,y) - I_i(\xi,y)}{I_S} = \frac{\lambda_P}{\lambda_L}\frac{\alpha_P P_{inc}\Theta(y)}{WLI_S}\int_0^L ds\exp\left[-\alpha_p\left|x(\xi,s)\right|\right] \tag{4}$$

The double-pass model can be readily derived from Eqs. (1-3), requiring that the forward-travelling intensity equals the backward-travelling intensity at $s = L$. We assume that, after the first pass, the beam retraces its path backward through the amplifier. Eventually, we end up with two equations, one for the single-pass ($q = 1$) and one for the double-pass amplifier ($q = 1/2$):

$$q \ln\left[\frac{I_o(\xi,y)}{I_i(\xi,y)}\right] + \frac{I_o(\xi,y) - I_i(\xi,y)}{I_S} = \frac{\lambda_P}{\lambda_L}\frac{\alpha_P P_{inc}\Theta(y)}{WLI_S}\psi(\xi) \tag{5}$$

where

$$\psi(\xi) = \frac{2}{\alpha_P \theta}\left[1 - \cosh(\alpha_P \xi)\exp\left(-\frac{\alpha_P \theta L}{2}\right)\right] \tag{6}$$

Notice that the small-signal gain coefficient is proportional to the right-hand side of Eq. (5): it is assumed to have a flat-top profile in the vertical direction while it has a smooth symmetric profile in the horizontal ξ-direction, with a peak on axis. This is a consequence of the bounce occurring at the mid-point of the slab. Moreover, thermal distortions that usually accompany the pump deposition are averaged accordingly, yielding the same symmetry as for the gain distribution along the ξ axis. Thermal lensing retains the usual distribution along the y axis.

As anticipated, an arbitrary seed beam profile can now be traced along the amplifier with Eqs. (5) and (6).

A particularly handy approximation, that speeds up the calculations significantly, consists in assuming an average gain coefficient over the horizontal seed diameter:

$$\overline{\psi} = \frac{2}{w_s}\int_0^{w_s/2}\psi(\xi)\,d\xi = \frac{2}{\alpha_P \theta}\left[1 - \frac{2}{\alpha_P w_s}\sinh(\alpha_P w_s/2)\exp\left(-\alpha_P \theta L/2\right)\right] \tag{7}$$

Rather than the transverse intensity distribution of the rays with coordinates (ξ,y), the spatially-averaged Eq. (5) yields now a single output intensity, given the seed cross section $w_s \times W$ and the input intensity:

$$q \ln\left[\frac{I_o}{I_i}\right] + \frac{I_o - I_i}{I_S} = \frac{\lambda_P}{\lambda_L}\frac{\alpha_P P_{inc}}{WLI_S}\overline{\psi} \tag{8}$$

It is worth noticing that the crystal end faces limit the effective width of the input seed. The beam width may be comparable with the distance between the centre of the beam and the edge of the slab input face, i.e. $\theta L/2$. On the other hand, when increasing the angle θ there is a possibility that the beam width becomes comparable with its distance from the other edge of the slab, of width D. Therefore, the effective beam diameter to be amplified is the minimum out of the quantities w_S, θL and $2(D\text{-}\theta L/2)$.

2.2 Amplification in pulsed, low-frequency regime ($f \ll 1/\tau$)

In pulsed amplification regime, usually a pulse-picker selects a single pulse from a cw mode-locked laser and sends it to the amplifier which was previously pumped to achieve an appropriate gain level. Assuming pump pulse duration T, and averaging the spatial gain distribution as in Eq. (7), the pump rate equation yields the small-signal exponential gain:

$$\frac{dn}{dt} = R_P - \frac{n}{\tau} \tag{9}$$

$$g_0 = \left\langle \int_0^L \sigma n \, ds \right\rangle = \frac{2}{w_s} \int_0^{w_s/2} d\xi \left[\int_0^L \sigma n(\xi, s) \, ds \right] = \sigma R_p \tau \left(1 - e^{-T/\tau}\right) \overline{\psi} \tag{10}$$

$$g_0 = \frac{\lambda_P}{\lambda_L} \frac{E_{inc}}{WLF_S} \frac{\tau}{T} \left(1 - e^{-T/\tau}\right) \overline{\psi} \tag{11}$$

We may now use the Franz-Nodvik amplifier model (Franz & Nodvik, 1963) to calculate the output fluence F_o, given the input fluence F_i and the amplifier saturation fluence $F_S = h\nu/\sigma$:

$$F_o = F_S \ln\left[1 + e^{g_0} \left(e^{F/F_S} - 1\right)\right] \tag{12}$$

So far we have considered amplification in a single slab. However, the output fluence from the first slab may be used as the input for a second pass or to the next slab, and so on, allowing in general different beam sizes and grazing angles to be considered for each stage of the amplifier chain.

2.3 Amplification in pulsed, high-frequency regime ($f \gtrsim 1/\tau$)

This operating regime is mostly employed in laser systems for industrial applications, where high processing speed is extremely important, even at the expense of some pulse energy reduction. In this case a cw pump laser is chosen owing to duty-cycle limitations of more powerful qcw laser diode arrays employed at lower frequency (typically $< 1/\tau$).

The amplifier gain (or the inversion population) between two amplified pulses is still restored according to Eq. (9), starting from the gain g_f just after the amplified pulse and reaching g_i just before the next seed pulse enters the amplifier.

The Franz-Nodvik model can still be used, provided we use the right initial gain, which, in turns, depends on the pulse repetition frequency (Koechner, 2006):

$$F_o = F_S \ln\left[1 + \left(e^{F/F_S} - 1\right) e^{g_i}\right] \tag{13}$$

$$g_i = g_\infty - \left(g_\infty - g_f\right) e^{-\frac{1}{f\tau}} \tag{14}$$

$$F_o = F_i + \left(g_i - g_f\right) F_S \tag{15}$$

We notice that, according to Koechner's notation, $g_\infty = \lim_{f \to 0} g_i(f)$ hence we identify $g_\infty = g_0$ as given in Eq. (11).

Again, Eqs. (13-15) apply to single-pass amplification, but sequential application of the same model readily accounts for multi-pass schemes or amplifier chains.

2.4 Bandwidth limitation and gain narrowing

The most important of limitations arising from the finite bandwidth of the amplifier concern single- or multi-pulse amplification in pulsed regime, when small-signal gain is very high,

say > 1000. This situation is commonly encountered in regenerative and multi-pass amplifiers (Walker et al., 1994; Le Blanc et al., 1996). However, single-pass amplification in a couple of grazing-incidence Nd:YVO_4 slabs readily yields 60 dB overall small-signal gain, leading to severe pulse broadening if too short seed pulses are injected.

In order to predict this effect quantitatively, we developed a numerical model based on Franz-Nodvik equations, adding gain filtering (of lorentzian form with fwhm = $\Delta\nu_g$) on each of the M slices into which the amplifier is sectioned. The basic assumption is that the gain depletion in each slice must be small enough (< 1%), so that we may apply the exact gain-filter model:

$$\hat{u}_{n+1}(\nu) = \hat{u}_{n+1}^{(u)}(\nu)\exp\left[\frac{(g_{n+1}+g_n)}{2}\frac{\gamma(\nu)}{2}\right] \tag{16}$$

$$\gamma(\nu) = \frac{1}{1+\left(2\nu/\Delta\nu_g\right)^2} \tag{17}$$

$$u_n(t) = \int_{-\infty}^{+\infty}\hat{u}_n(\nu)e^{-i2\pi\nu t}\,d\nu \tag{18}$$

where $\hat{u}_{n+1}^{(u)}(\nu)$ is the Fourier transform of the amplified (unfiltered) field $u_{n+1}^{(u)}(t)$ at the end of the (n+1)-th section, according to the Franz-Nodvik model:

$$G_{n+1} = \frac{e^{E_n/E_s}}{e^{E_n/E_s}-1+1/G_n^{(0)}} \tag{19}$$

$$E_n = \int_{-\infty}^{+\infty}\left|u_n^2(t)\right|dt \tag{20}$$

$$G_n^{(0)} = G_0^{1/M} \tag{21}$$

$$g_n = \ln(G_n) \tag{22}$$

Here G_0 is the total small-signal gain, and g_n is the result of the previous step. The condition for accurate computation is that

$$\frac{g_n - g_{n+1}}{g_n} \ll 1 \tag{23}$$

Therefore M is chosen accordingly. We notice that computation time might be conveniently reduced provided one chose a logarithmic distribution of amplifier sections lengths, since most severe saturation occurs at the end of the amplifier. However, in order to model amplifier gains as high as 60 dB, we found that M = 500 yields sufficiently accurate results with only few seconds of computation time on a 2.4-GHz laptop.

Let us consider typical data for a pulsed grazing-incidence amplifier: $\Delta\nu_g$ = 212 GHz (*a*-cut Nd:YVO_4, fluorescence fwhm = 0.8 nm (Zayhowski & Harrison, 1997)), F_S = 125 mJ/cm² and E_S = 188 μJ. We calculated the output energy and pulse width as a function of small-signal gain, input energy and seed pulse width. The results are summarised in Figs. 2-4.

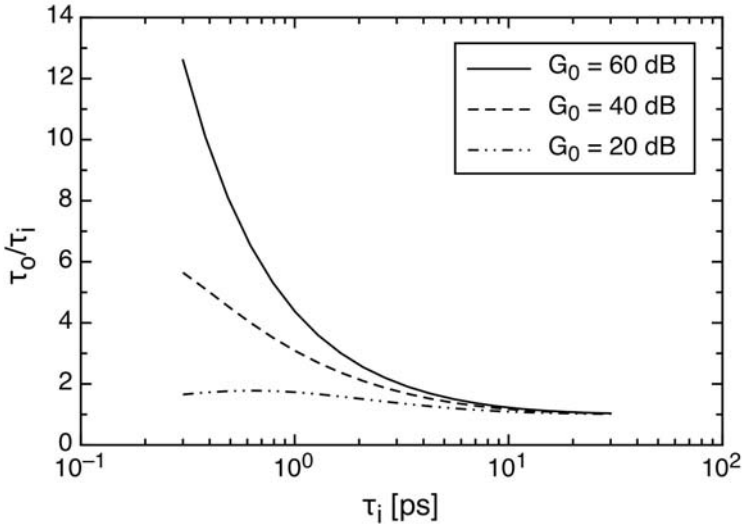

Fig. 2. Output pulse width broadening as a function of the seed pulse duration. Three small-signal gain levels are considered. Injected seed energy of 1 nJ is typical of most picosecond seeders.

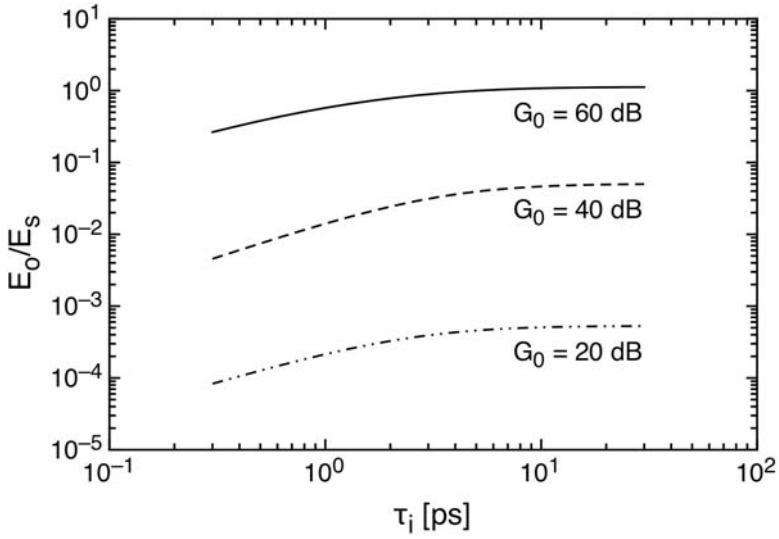

Fig. 3. Output energy as a function of the seed pulse width, for three small-signal gain levels. Injected seed energy is 1 nJ.

In conclusion, we note that seed pulse duration exceeding four times the minimum width set by the amplifier bandwidth (≈ 1.5 ps in this example, assuming *sech*² pulse shape) produces no significant broadening after amplification even at an unsaturated gain of 60 dB (Fig. 2). The gain narrowing effect is most clearly seen at shorter seed pulse widths, as expected. Notice that at relatively low gain values, G_0 < 20 dB, the output pulse width reaches a maximum broadening as the seed pulse shortens, then approaches the seed duration provided it is short enough. The physical explanation is that the gain modulation is not as strong as with higher gain, so that only a relatively small central region of the seed spectrum is amplified but the overall non-amplified spectrum energy dominates, leading to an output pulse width still approaching that of the seed pulse.

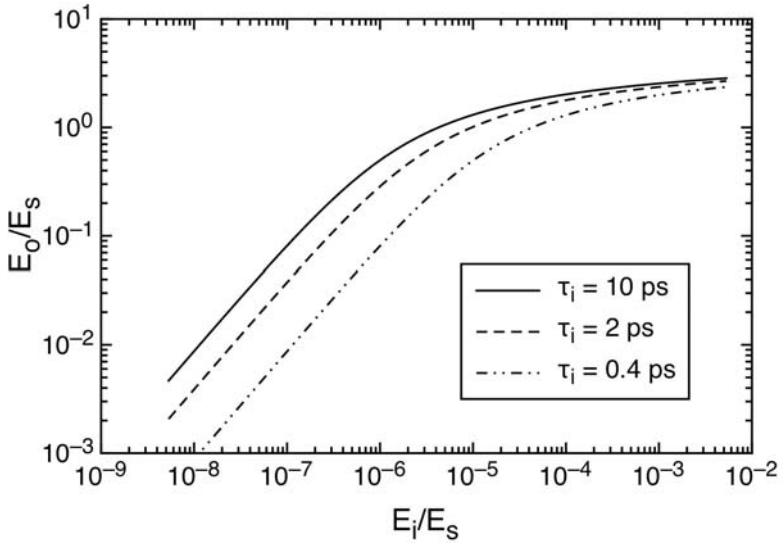

Fig. 4. Output energy as a function of the seed energy (both normalised to the saturation energy); three different seed pulse width have been considered.

As far as efficient energy extraction is of concern, Fig. 3 shows that with the given (typical) amplifier parameters a small-signal gain G_0 = 50-60 dB is required to reach saturation starting from the typical seed energy level ≈ 1 nJ. It is remarkable that, whilst this is usually achieved with either regenerative or extra-cavity multi-pass setups, typical gains of qcw grazing-incidence modules ≈ 30 dB/slab yield such gain levels with only two slabs or a single slab in two-passes, if only one is careful enough to suppress ASE.
Fig. 4 shows that gain saturation in the Nd:YVO_4 slab is optimised with seed pulse width > 6 ps: this means that, owing to gain narrowing, all the seed spectral energy is used for the effective amplification bandwidth.

2.5 Temporal distortions from amplifier saturation

This effect is most relevant when amplifying relatively long pulse trains, typically with an envelope duration > 50 ns for G_0 ~ 60-70 dB. It originates from the strong amplification experienced by the leading edge of the train envelope, which depletes the gain reducing the amplification of the trailing edge of the envelope.

The distortion can be readily calculated from the Franz-Nodvik model, given the power envelope *P(t)* of the pulse train, the small-signal gain G_0 and the saturation energy E_S:

$$G(t) = \frac{e^{E_i(t)/E_s}}{e^{E_i(t)/E_s} - 1 + 1/G_0} \tag{24}$$

$$E_i(t) = \int_{-\infty}^{t} P_i(t')dt' \tag{25}$$

$$P_o(t) = G(t)P_i(t) \tag{26}$$

Therefore, the envelope modulation waveform required for pre-compensation of the saturation distortion can be easily computed, in order to yield a nearly flat-top output pulse from the amplifier. Owing to the strong amplifier saturation, the output energy reduction due to the pre-compensation is not very penalizing, notwithstanding the significant energy reduction of the modulated seed. This will be discussed in more detail in Section 5.

3. Amplification of a cw picosecond laser

Here we discuss the simplest setup that one can conceive, i.e. a single grazing incidence slab, side-pumped by a single diode array, for amplification of a low-power cw picosecond laser. In particular, the seeder is a Nd:YVO_4 oscillator (Fig. 5), longitudinally pumped by a 1-W laser diode at 808 nm. The laser is passively mode-locked with a SESAM, generating a 50-mW average power train of 6.8-ps, linearly polarized pulses at a 150-MHz repetition rate in each of the two diffraction-limited output beams.

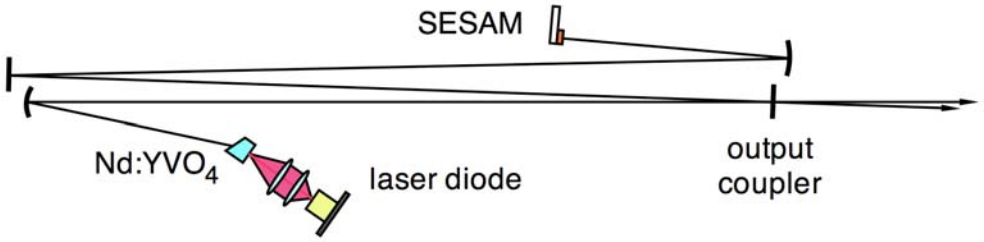

Fig. 5. Representative layout of a cw diode-pumped picosecond oscillator.

A 4 x 2 x 16 mm^3, *a*-cut, 6°-wedged, 1%-doped Nd:YVO_4 slab is employed as amplification head, pumped by a TE-polarised 10-mm x 1-µm laser diode array, emitting at 808 nm and collimated along the fast-axis by a 0.9-mm focal length microlens. This laser diode is actively cooled and temperature controlled with a thermoelectric cooler and emits a beam of maximum power of 32 W. The amplifier crystal is antireflection (AR) coated at 1064 nm on the input and output faces and simply polished and uncoated on the pumped side face. The Fresnel loss of about 14% of the incident pump power limits the absorbed pump power at 28 W. The 4 x 16 mm^2 slab faces are placed in contact with a water-cooled heat exchanger by thin indium foils. A proper choice of the water temperature set point is crucial in optimising the amplifier performances. The reason is twofold: i) minimisation of the thermal stress

inside the slab and ii) reduction of the thermal red-shift of the fluorescence bandwidth of Nd:YVO_4, that may reduce the amplifier gain and performance. In this case the optimum operating temperature is 8°C. The collimated beam emitted by the pump diode is polarisation-rotated by a half-wave plate and focused into the Nd:YVO_4 slab with a 15-mm focal length cylindrical lens.

In order to estimate the vertical thickness of the gain sheet, the seed beam is collimated (0.9-mm half-width at $1/e^2$) and sent to the amplifier without any focusing optics. In these conditions, because of the strong gain shaping of the pump beam in the high-gain amplifier and of the great mismatch between the seed diameter and the gain-sheet thickness, the beam divergence along the y-direction is nearly pump-insensitive. Considering a flat-top y-profile for the output beam leaving the amplifier, the thickness W of the gain-sheet can be readily estimated by measuring the full vertical divergence angle $\theta_y \approx 2\lambda_L/W$. In this example it turns out $W \approx 70$ µm. Notwithstanding the clearly non optimised beam size, the seed beam yields up to 3.5 W in a single pass through the amplifier for an optimum internal grazing-incidence angle of ≈ 3°.

The setup for the cw amplification experiments is shown in Fig. 6.

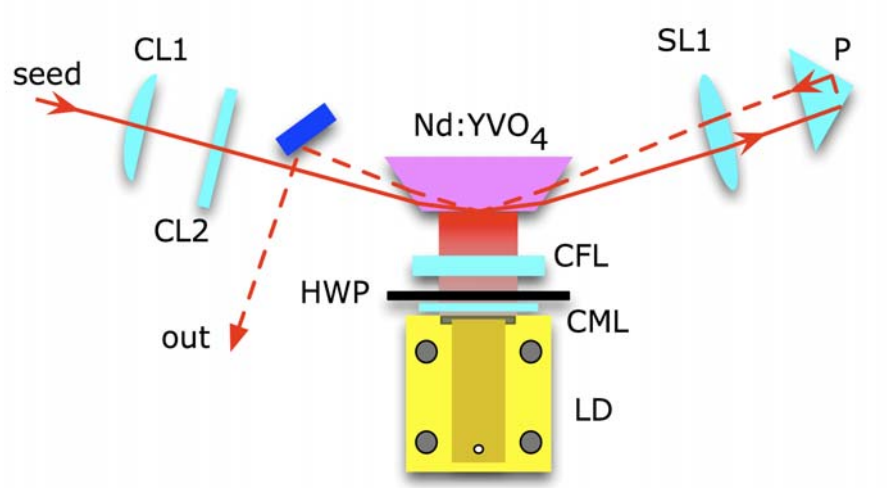

Fig. 6. Setup for the cw amplifier. CL1: 250-mm focal cylindrical focusing lens; CL2: 100-mm focal cylindrical focusing lens; SL1: 200-mm focal spherical lens; P: right-angle prism; CFL: 15-mm focal cylindrical pump focusing lens; HWP: half-wave plate; CML: collimation microlens (0.9-mm focal length).

Being the thickness W of the gain sheet set by the pump focusing lens and limited by the residual smile of the laser diode, the depth of the gain sheet in the horizontal plane is basically determined by the pump absorption depth, $1/\alpha_P \approx 0.5$ mm, given the typical pump spectrum width (≈ 2-3 nm) and the 1%-doping concentration of Nd:YVO_4. This generates an elliptical transverse gain profile that suggests the need for a different seed focusing in the horizontal and vertical directions. As shown in Fig. 6, the cylindrical lens CL1 focuses the oscillator beam down to $w_x \approx 100$ µm in the horizontal plane, whereas a cylindrical lens CL2 focuses the seed beam in the vertical plane to $w_y \approx 36$ µm. In order to choose the seed waist

inside the amplifier, both the thickness of the pumped region and the Rayleigh range of the focused beam should be taken into account. In particular the pumped region length along the seed propagation direction should be shorter than two times the Rayleigh range of the focused beam in order to take advantage of the entire length of the active region. These considerations set a minimum acceptable dimension of ≈ 30 μm for the focused seed beam waist. Moreover, the grazing incidence angle has to be chosen as small as possible in order to maximise the gain while avoiding clipping effects.

With 34-mW seed injection the amplifier yields as much as 6.1 W after a single pass for the 28-W absorbed pump power, corresponding to a 22% optical-to-optical efficiency. The beam quality of the seed ($M^2 = 1.1$) is only slightly degraded to $M_x^2 = 1.3$ and $M_y^2 = 1.2$ at the maximum amplification level.

Fig. 7 shows the autocorrelation traces of both seed and amplified pulses and the correspondent optical spectra. The pulse duration after amplification is only slightly increased and the effect of spectral gain narrowing is quite evident. We notice that, owing to dishomogeneous broadening due to spatial hole burning (Flood et al., 1995), longitudinally-pumped picosecond lasers with gain at the end usually show excess bandwidth with respect to the measured pulsewidth. Therefore, in this case gain narrowing improves the pulsewidth × bandwidth product from 0.68 for the seed to 0.42 for the amplified pulses, approaching the Fourier limit of 0.32 for a *sech*² pulse shape.

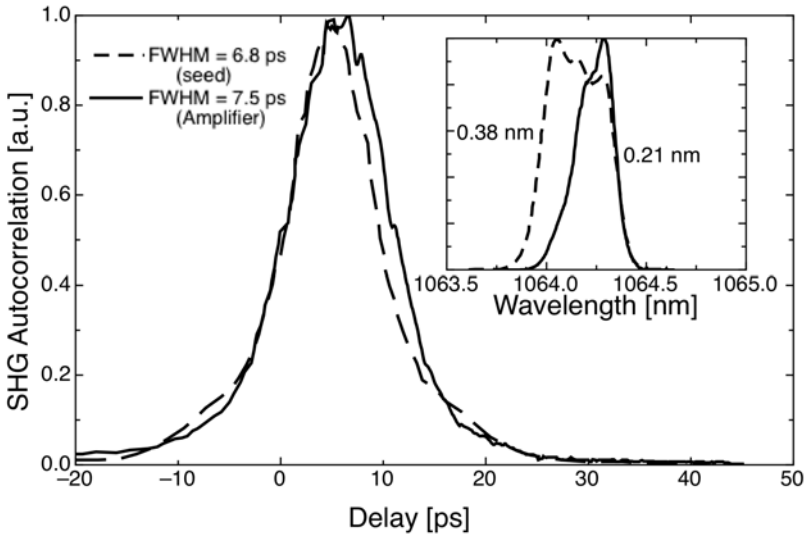

Fig. 7. Pulse autocorrelation of seed (dashed curve) and amplified (continuous curve) beam. Inset: corresponding optical spectra for seed and amplified pulses.

Double-pass amplification can be conveniently realised by re-imaging the single-pass output with a spherical lens SL1 (200-mm focal length) and a right-angle antireflection-coated prism P (see Fig. 5), thus maintaining the same spot size as in the first pass, but with a slightly increased grazing angle of ≈ 4°. Beam extraction occurs before the lens CL2.

The first consequence of realising a return path in the amplifier is the immediate growth of the amplified spontaneous emission (ASE) background. When the pump diode beam is

focused for single-pass amplification, addition of the second pass boosts the ASE to > 1 W in this setup. In order to reduce the gain in the amplifier and hence the amount of ASE, the pump diode focusing must be relaxed, for example replacing the 15-mm cylindrical lens with a 20-mm lens.

This increases W to ≈ 95 μm. In these conditions ASE background reduces to < 200 mW and as much as 8.4 W are obtained at 28-W absorbed pump power after second pass amplification. The corresponding optical-to-optical efficiency increases to ≈ 30%.

Owing to a relatively small horizontal beam width compared to the horizontal transverse gain profile dimension, off-axis thermal aberrations in the critical horizontal plane are reasonably low. Therefore beam quality is well conserved also after the second pass ($M_x^2 = 1.4$ and $M_y^2 = 1.3$). Results similar to those reported in Fig. 7 are obtained for both pulse autocorrelation and spectrum.

Several different configurations were investigated, in single and double pass and also employing a single 300-mm focal spherical lens to focus the seed into the Nd:YVO_4 slab instead of the cylindrical optics shown in Fig. 6. Both the amplifier gain as a function of the injected seed power and the output power as a function of the absorbed pump power are summarised in Figs. 8 and 9.

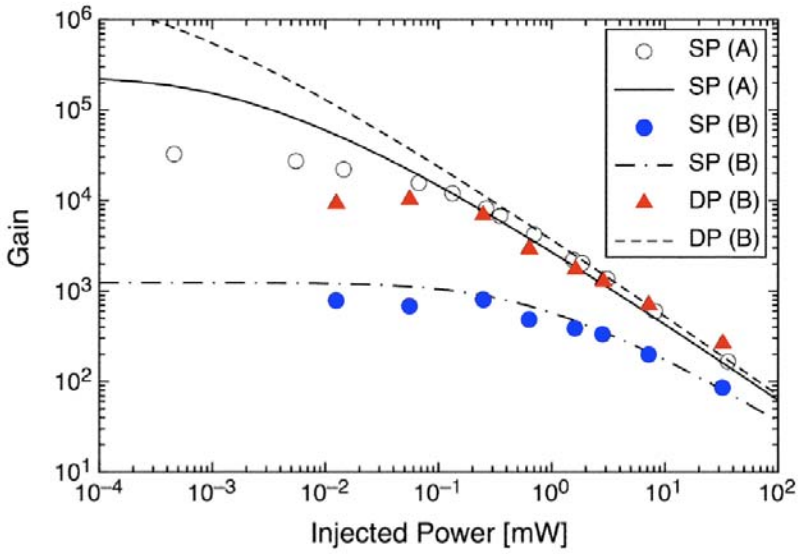

Fig. 8. Gain curves for the single- and double-pass amplifier. (A) Setup with pump focusing with 15-mm focal and seed focusing with cylindrical lenses of focal lengths f_x = 250 mm and f_y = 100 mm. (B) Setup with pump focusing with 20-mm focal and seed focusing with 300-mm focal spherical lens. SP single pass, DP double pass. Continuous curves: numerical results. Points: data.

Both in single or double pass setup, a small signal gain higher than 40 dB for the lowest input power is obtained. The model employed for fitting the experimental data is described

in Section 2.1. The following physical parameters of the laser crystal can been used to fit the experimental data: $I_S = 2$ kW/cm^2, $\alpha_{P0} = 24$ cm^{-1}, $I_{SA} = 3.61$ kW/cm^2. The unsaturated absorption coefficient has been calculated assuming the absorption spectrum averaged over the laser diode emission spectrum. The best-fit saturation intensity value I_S yields a product $\sigma\tau$ about 30% smaller than the one usually reported in literature. Such a behaviour, beside intrinsic model approximations, can be explained by a reduction of the fluorescence lifetime due to up-conversion effects and by a reduction of the effective emission cross section due to the mismatch between the spectrum peaks of seed and amplified pulses (see the inset of Fig. 7).

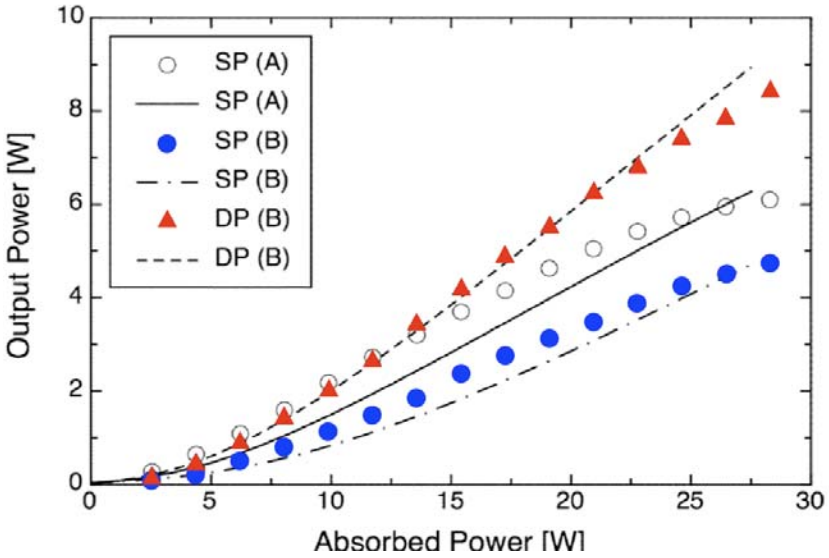

Fig. 9. Output power as a function of the absorbed pump power for the single- and double-pass amplifier. (A) Setup with pump focusing with 15-mm focal and seed focusing with cylindrical lenses of focal lengths $f_x = 250$ mm and $f_y = 100$ mm. (B) Setup with pump focusing with 20-mm focal and seed focusing with cylindrical lenses $f_x = 250$ mm and $f_y = 100$ mm. SP single pass, DP double pass. Continuous curves: numerical results. Points: data.

As clearly shown by Fig. 8, the amplifier behaviour tends to deviate from the model for decreasing injected power levels, suggesting that the maximum available gain is lower than that predicted. For very small injected power, gain saturates around $\approx 10^4$ owing to ASE, while gain saturation with higher input seed power levels recovers a fair agreement between predictions and experiments, since stored energy is more effectively extracted from the amplified beam rather than being wasted into wide-angle ASE.

4. Single-pulse amplification up to 1 kHz repetition rate

A typical, representative layout of a laser system for single picosecond pulse amplification after pulse-picking is shown in Fig. 10.

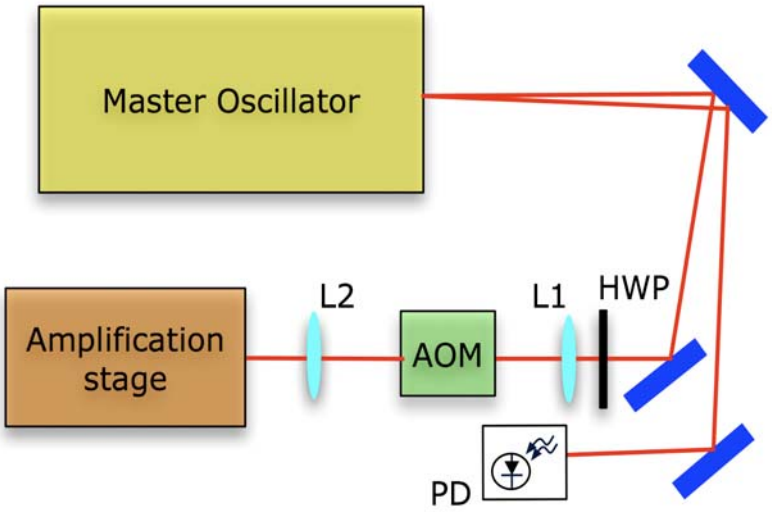

Fig. 10. Layout of a laser system for single pulse amplification. HWP: half-wave plate; L1: focusing spherical lens; L2: collimating spherical lens; AOM: acousto-optic modulator; PD: photodiode.

The master oscillator in this case is still similar to that used for cw experiments, providing two output beams each carrying out about 70-mW average power, 7.7-ps long pulses but with a reduced repetition rate ≈ 48-MHz. This last parameter is important since well-separated pulses are easier to pick up with optoelectronic devices.

The repetition frequency downscaling scheme for single pulse amplification employs an acousto-optic modulator (AOM) to pick up single pulses from the cw mode-locked oscillator. The major benefit of using AOM with respect to faster electro-optic modulators for pulse picking is the simpler and easier to customise driving electronics. Moreover AOMs are cheaper and do not require fast switching of high voltages that generates electromagnetic noise difficult to suppress. The pulse train sampled by the pulse picker has programmable repetition frequency, basically upper-limited by the duty cycle of the high-power diode arrays pumping the amplifier stage, that is typically 10%. In case of vanadate slab amplifiers, since the fluorescence time is ≈ 100 μs, the maximum operating frequency for qcw laser diodes bars is fixed at 1 kHz.

Given a temporal separation between two adjacent master oscillator pulses larger than the minimum deflection window allowed by the AOM, the key issues is to be able to drive the pulse picker synchronously with respect to the laser pulses. The correct timing can be realised conveniently by employing one of the two beam outputs from the master oscillator to generate a clock signal intrinsically synchronous to the pulse train for the pulse-picker driving electronics. In this example, a time separation between two adjacent pulses of about 20 ns allows a suppression ratio between selected and adjacent pulses better than 2% with a deflection efficiency exceeding 40%. If higher suppression ratio were an issue, a faster pulse picker, two acousto-optic pulse pickers in series or an oscillator running at a lower repetition rate might be employed.

The amplification stage setup is shown in detail in Fig. 11. The seed emerging from the pulse picker is injected into a grazing-incidence single-pass amplifier made by a couple of 4 x 2 x 16 mm^3, *a*-cut, 5°-wedged, 1%-doped Nd:YVO_4 slabs. The slabs are AR-coated at 1064 nm at the input and output faces, while the pumped sides are AR-coated at 808 nm. Each slab is pumped by a 150-W peak power qcw laser diode array with an emitting size of 10 mm x 1 µm. The radiation emitted by each diode is collimated by a microlens to ≈ 0.9-mm thickness x 10-mm width stripe and polarisation rotated by a half-wave plate to be aligned with the *c*-axis of the vanadate slabs. Notice that, owing to the much higher peak power of the diode arrays, tight focusing into the slab is no more required as in the cw amplifier of Section 3.

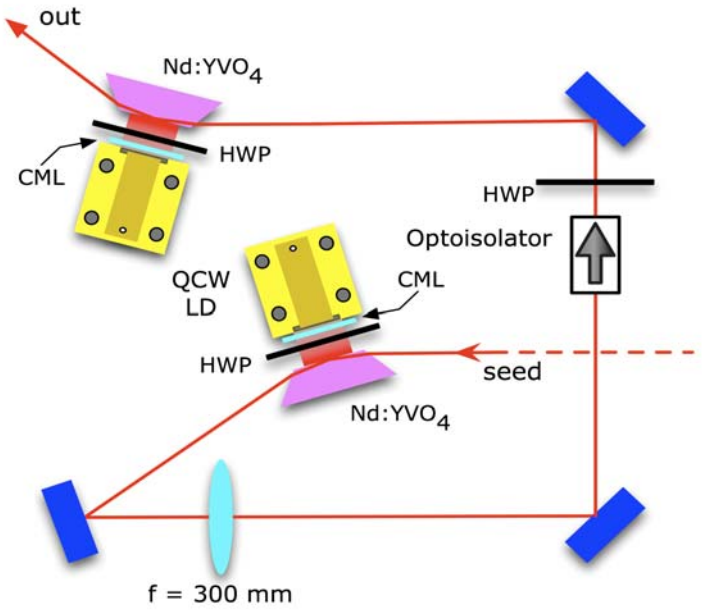

Fig. 11. Setup for the single-pulse amplification 2-slabs module. HWP: half-wave plate; CML: collimation microlens (0.9-mm focal).

In order to optimise the energy storage in the amplifiers the pump pulse duration is set to about 100 µs, slightly longer than the fluorescence time of the 1%-doped Nd:YVO_4 slab. The pulse picking occurs on the trailing edge of the pump current pulses, when the maximum gain is stored in the amplifiers medium.

Pulse duration is slightly increased after amplification. As shown in Fig. 12, fwhm 7.7-ps long seed pulses are slightly stretched to 11 ps long. The 0.37-nm wide pulse spectrum is substantially preserved during amplification, improving the quality parameter pulsewidth × bandwidth.

In order to fully exploit the potential of high-gain amplifier modules, besides the optimisations concerning the grazing angle as well as the matching between the seed beam waist and the gain layer, the main issue is to be able to contrast successfully those effects, such as amplified spontaneous emission (ASE), that compete with the amplifying beam in depleting the population inversion in the gain media. Since the ASE generated in the one

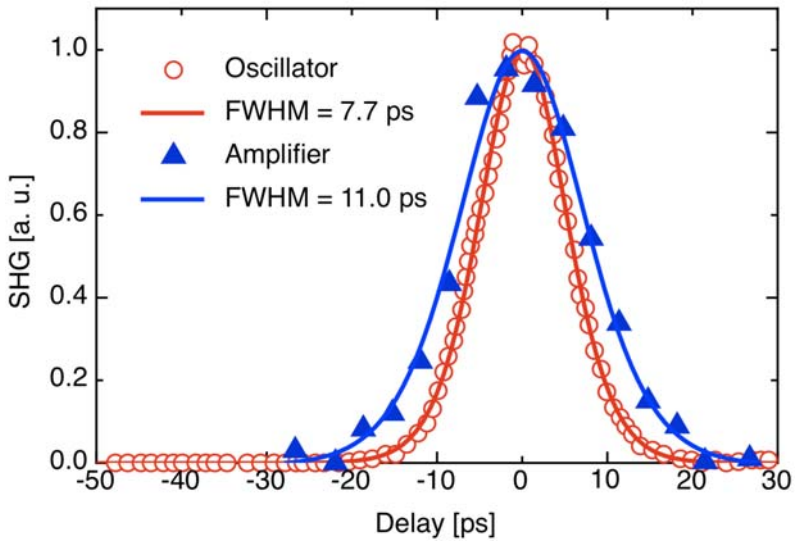

Fig. 12. Pulse autocorrelation of the oscillator (circles) and amplified (triangles) beam. Also shown are the best-fit traces corresponding to *sech*² intensity envelope.

slab can seed the other, the two amplifiers must be kept sufficiently separated, about 30 cm in the final setup, in order to reduce the solid angle under which the first slab is seen by the second and consequently reduce the reciprocal ASE seeding. This solution yields significant performance improvements with respect to more closely separated slabs only few centimetres apart (Agnesi et al., 2006b). Furthermore, an optical isolator is inserted between the two amplifiers to prevent self oscillations and back-injection in the direction of the master oscillator. A spherical lens (300-mm focal length) placed at about 250 mm from the second slab re-collimates the spatial mode before entering the second amplifier.

A small-signal gain as high as $\approx 10^6$ ($\approx$ 60 dB) is measured for this double-slab module. Injecting pulses with energy of about 0.4 nJ, yields amplified pulses with energy as high as 210 μJ with weak gain saturation. Fig. 13 shows the energy extraction curve of the amplifier.

The model for experimental data fitting is described in Section 2.2. The following best-fit parameters values can be employed: saturation fluence F_S = 133 mJ/cm² (correspondent effective emission cross-section $\sigma \approx 15 \times 10^{-19}$ cm²), absorption coefficient α_P = 22 cm^{-1}, gain thickness W = 1.2 mm (flat-top approximation). For the seed beam it is assumed an equivalent flat-top profile diameter w_s = 0.6 and 0.8 mm in the first and second slab respectively, while the grazing incidence angle θ is 1.6° in both slabs, according to a direct measurement of the deviation angle at the slabs output for the configuration yielding the highest pulse energy. The calculated angular sensitivity of the second amplifier is shown in Fig. 14. The model confirms that the slab amplifiers are operated near the optimum predicted angle.

Moreover, the numerical model suggests some useful optimisation criteria for further improvements of the system performances. First of all, in order to fully exploit the gain available in the first slab it is necessary to reduce the transverse dimensions of the seed beam in order to match its confocal parameter with the length of the pumped region. Such a relatively small beam size allows to explore smaller grazing incidence angles without

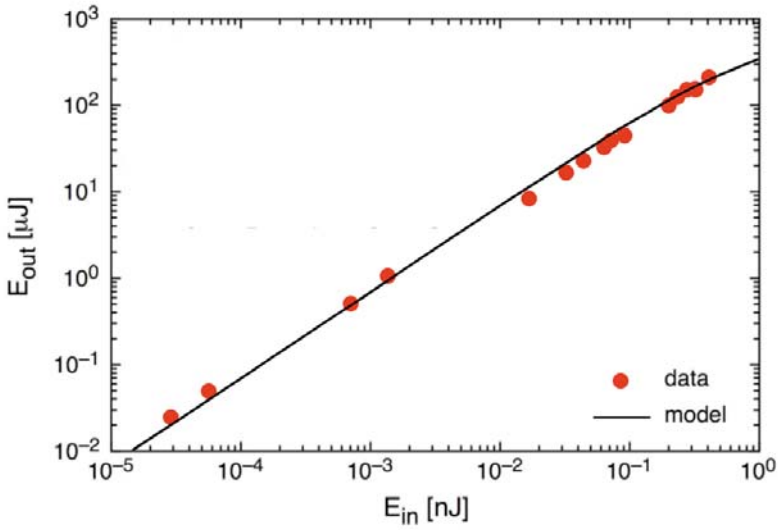

Fig. 13. Energy extraction curve of the amplifier (experiment and numerical model).

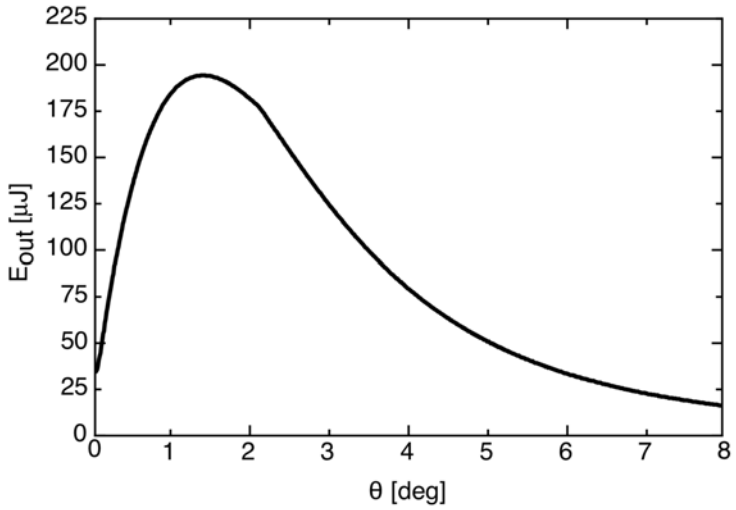

Fig. 14. Calculated energy extraction curve of the second amplifier as a function of the grazing incidence internal angle θ corresponding to a full pump power and maximum seeding injection.

clipping the beam, hence maximising the small-signal gain in the first unsaturated amplifier. Beam clipping should be carefully avoided, since it produces scattering and beam distortions that can substantially limit amplifiers performance. In the second slab the beam

transverse dimensions and the grazing incidence angle should be increased in order to reduce non-linear effects and damage issues. The upper limit to input beam waist is given in this case by the gain region thickness *W*. According to these guidelines, output energy is predicted to increase up to 0.5 mJ with very small grazing incidence angles (≈ 0.3°) in the first slab and beam radius ≈ 0.5 mm in the second slab.
It is worth noticing that for an accurate measurement of the output pulse energy it is necessary to remove the contribution of both ASE and undesired background pulses. In fact, since the static extinction ratio of the AOM is ≈ 1:2000, this value can be considered the attenuation factor for pulses far away from the selected one, while pulses coming immediately before and after the selected one will surely experience an even lower extinction ratio. All of these contributions can become significant after amplification and affect a direct measurement carried out with a power meter. However, the post-amplification pulse contrast will be significantly increased by second harmonic generation (SHG), since the integrated contribution of the small background pulses will be practically negligible and the only significant contribution will come from the main pulse. Following these considerations, the amplified pulse energy at the fundamental wavelength can be inferred from a measurement of both SHG conversion efficiency and second harmonic pulse energy. With this setup it was obtained up to 160 μJ at 532 nm with a conversion efficiency of 75% in an angularly phase-matched 3 x 3 x 8 mm^3, type-I LiB_3O_5 (LBO) crystal without any focusing, owing to the high peak intensity level (≈ 4.8 GW/cm^2) of the nearly diffraction-limited amplified picosecond pulses. Fourth harmonic generation was also performed, employing the SHG pulse as the pump for a 3 x 3 x 7 mm^3 β-BaB_2O_4 (BBO) crystal. As much as 64 μJ at 266 nm were generated with 40% conversion efficiency.
The high peak power makes such laser sources ideal for simple, travelling wave optical parametric generation (OPG). With only 10 μJ at 1064 nm, 55%-efficiency SHG in a 15-mm LBO crystal yields ≈ 8-ps pulses at 532 nm for pumping an OPG, consisting in a 15-mm type-II $KTiOPO_4$ (KTP) for phase-matching in the *xz* plane. Tight focusing to ≈ 40-μm spot radius yields signal generation in the range 770-1020 nm (idler range was ≈ 1110-1720 nm) with angle tuning, with small efficiency ≈ 1%. This OPG might be readily amplified by a second stage pumped by a more energetic pulse at 532 nm, with much higher conversion efficiency and energy.

5. Amplification of high repetition rate pulse trains

Some applications requires amplification of bunches of pulses instead of single pulses or continuous trains. The repetition rate of the micro-pulses contained in the bunches is set by the master oscillator, while temporal shape, duration and repetition frequency of the micro-pulses envelope (macro-pulse) can be settled by a suitable pulse-picking device. High small-signal single-pass gain diode side-pumped grazing incidence amplifier modules can be employed also for macro-pulse amplification, owing to their good performances in terms of gain, beam quality and micro-pulse duration preservation, their relatively simple optical arrangement and their cost effectiveness.
The main issue, peculiar of this application, is related to the severe temporal distortions experienced by the envelope of the pulse burst during amplification, due to gain saturation and extremely high gain values. This effect is strongly dependent on the macro-pulse

duration and in the end limits the possibility to obtain rectangular-shaped amplified envelopes for macro-pulses longer than few μs or even few hundreds of ns, depending on the amplifiers saturation level. In order to overcome amplification distortions it is necessary to inject in the amplifier chain a conveniently shaped macro-pulse with a temporal envelope designed to compensate saturation effects (Butterworth et al., 1996). This can be done by modulating the radio-frequency driving signal of the AOM pulse picker. An example of rectangular-shaped and custom-shaped macro-pulses is shown in Fig. 15.

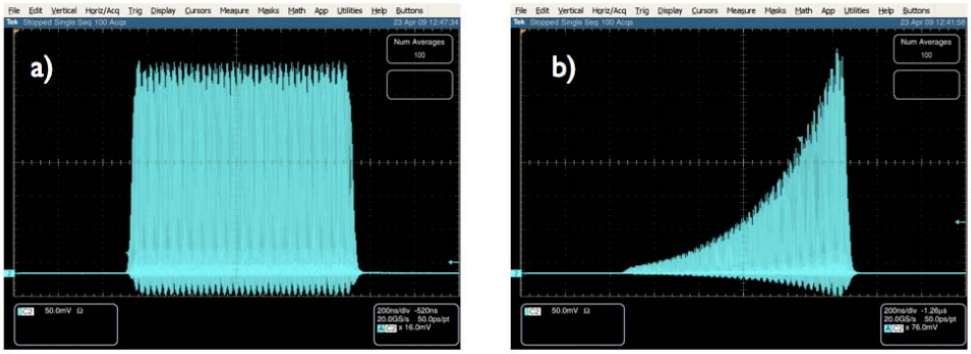

Fig. 15. Examples of two different deflected waveforms. a) Rectangular-shaped macro-pulse envelope; b) Macro-pulse envelope reshaped for amplification distortions compensation. Note that the energy of the modulated envelope is reduced to ~ 1/3.

In the example reported here, the master oscillator for pulse train amplification experiments is an high-frequency passively mode-locked Nd:YVO_4 oscillator (Agnesi et al., 2005). The ≈ 3-cm long V-folded resonator is pumped by a 1-W cw laser diode emitting at 808 nm, yielding ≈ 20-mW average power, ≈ 5-GHz repetition rate, 6-ps long mode-locking pulses.
The AOM pulse-picker yields typically 500-ns long macro-pulses containing approximately 2500 picosecond micro-pulses from the continuous train (any macro-pulse length > 50 ns can be chosen). The macro-pulses are amplified employing three Nd:YVO_4 slabs, as shown in Fig. 16.
Each 14 x 4 x 2 mm^3, *a*-cut, 1% doped vanadate slab is side-pumped by a pulsed 150-W peak power laser diode array. A couple of optical isolators are employed to prevent self-lasing and dangerous, high-intensity back-injections in the direction of the master oscillator. The deflected laser beam emerging from the acousto-optic modulator needs to be carefully collimated to a vertical dimension optimally matched to the pumped layer, while the path between the three amplification heads is kept sufficiently long in order to reduce the amount of ASE generated in the first amplifier and injected into the others. All these optimisations contribute to achieve a single-pass gain of ≈ 70 dB. As shown in Fig. 17, pulse duration increases from 6 ps to 8.9 ps after amplification.
A maximum output energy of about 2.5 mJ per macro-pulse is obtained after the three stage amplifier. The pulse spectrum after amplification is significantly narrowed: starting from a master oscillator 0.4-nm wide spectrum (fwhm), it shrinks to ≈ 0.19 nm at the output of the diode pumped amplifiers. Beam quality is well preserved ($M^2 \approx 1.2$) as Fig. 18 clearly suggests.

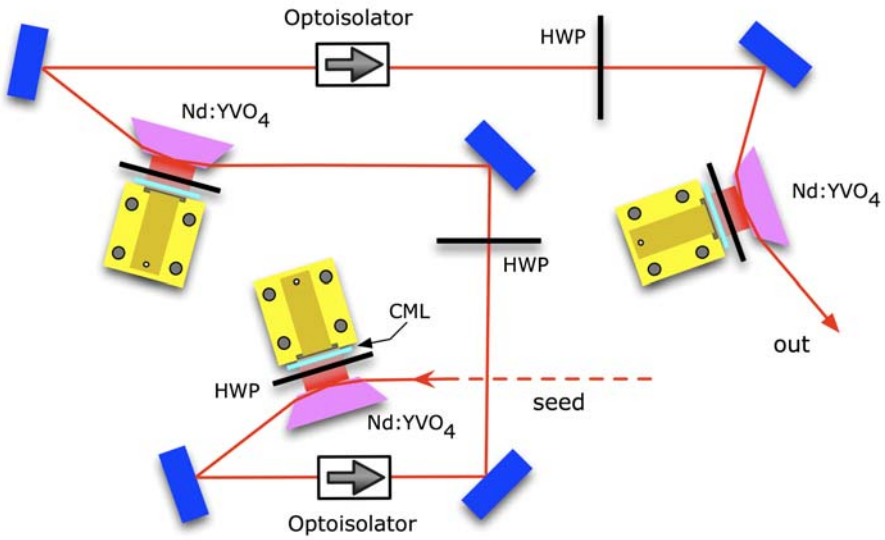

Fig. 16. Diode pumped amplifiers setup for pulse train amplification. Each laser diode beam is polarisation-rotated by a half-wave plate (HWP) and collimated by a 0.9-mm collimation microlens (CML).

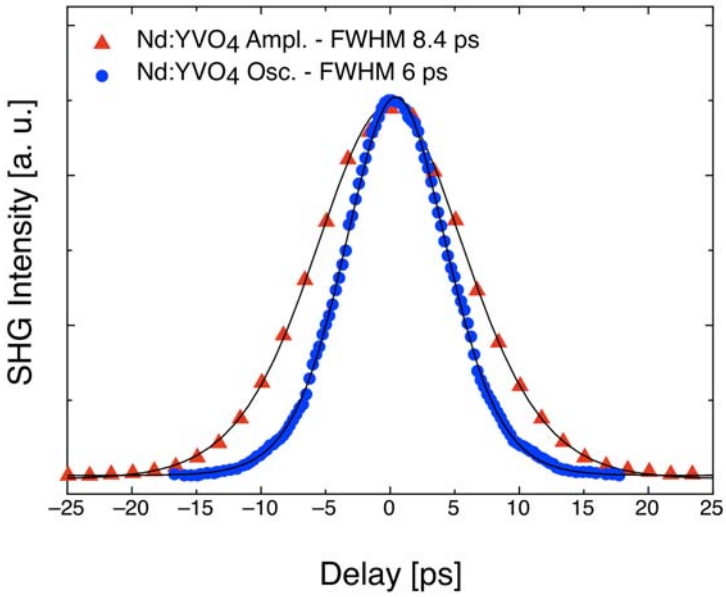

Fig. 17. Autocorrelation traces of both master oscillator (circles) and amplified pulses (triangles). Also shown the sech^2 experimental data fitting.

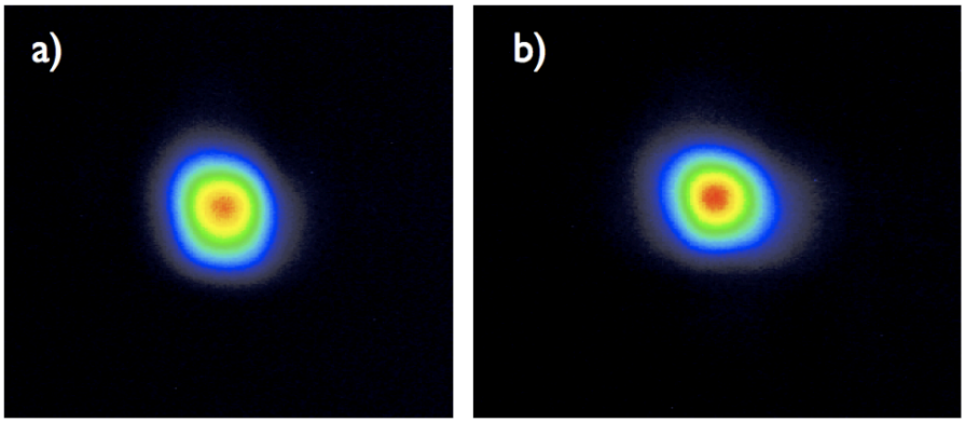

Fig. 18. Laser beam profile before amplification (a) and at the amplifier output (b).

Macro-pulse repetition rates up to 1 kHz can be chosen, owing to the duty cycle limitation of qcw diode arrays discussed previously.
A particular high-energy application required that the macro-pulses emerging from the diode pumped amplification stage was further amplified in a couple of 12-cm long, 6-mm diameter, flash-lamp pumped Nd:YAG rods.
At the maximum pump level, energy as high as 300 mJ was obtained for a 500-ns macro-pulse containing approximatively 2500, 12-ps long micro-pulses. The good beam quality ($M^2 = 1.5$) and peak power > 10 MW of the single pulses in the amplified burst allowed efficient nonlinear frequency conversion.
SHG efficiency as high as 60% at 532 nm was achieved in a 16-mm long type-I LBO crystal. The second harmonic output beam was used to synchronously pump an optical parametric oscillator (OPO) plane-plane cavity. The nonlinear medium was a 12-mm long AR-coated KTP crystal cut for type II phase-matching. Both the OPO mirrors and the crystal coatings were designed for singly-resonant oscillation around 800 nm, even though much broader tuning behaviour might be obtained in principle, with a suitable choice of mirror coatings. At the maximum pump energy at 532 nm, with a 40% transmitting output coupler the OPO generated about 60-mJ at 800 nm, in 500-ns long, rectangular-shaped macro-pulses.

6. Conclusions

Effective amplification of diode-pumped picosecond laser oscillators employing grazing-incidence side-pumped slab modules has been reviewed. Numerical models, useful for the design and the investigation of the amplifier characteristics, both in terms of energy extraction and pulse dynamics, have been illustrated. Some particularly representative examples of such amplification techniques, under various operating regimes, have been reported and discussed, comparing their results with the numerical model and putting them in perspective against other state of the art amplification schemes.
The most distinctive features of grazing-incidence amplifiers can be summarised as follows:

- extremely high gain that allows considerable setup simplification;
- strong gain shaping allowing beam quality preservation along the fast axis of the diode array, notwithstanding the strong thermal lensing in that direction;

- compactness, modularity and easy scalability.

It has been pointed out that picosecond laser amplification might be now take advantage of simple, rugged cw mode-locked fibre lasers, adding DPSS amplifiers such as grazing-incidence slabs. This is especially interesting for high-energy picosecond pulse amplification at multi-kHz up to MHz repetition rate.

Higher power and energy levels can readily be obtained by adding pump diodes or even diode stacks, instead of using a single diode array to pump the bounce face of the slab (Minassian et al., 2005).

Applications of this amplification technique can also be attractive for other laser materials such as Yb^{3+}-doped crystals (mostly Yb:YAG), Nd:glass, Nd:YAG and Nd:YLF. It is required that the absorption depth be small enough, and the absorbed pump power sufficiently high to produce a population inversion density yielding an integrated gain ≈ 20-30 dB per pass, in order to exploit all the useful features of the grazing-incidence slab. Particularly attractive are wide-band materials such as Nd:glasses that might allow high-energy femtosecond amplification with much simpler setups than usually reported in literature, at least using powerful qcw diode arrays at relatively low frequency (< 1 kHz). Quasi-three level materials such as Yb^{3+}-doped crystals also allow sub-picosecond and femtosecond amplification, however their re-absorption losses have to be taken into account properly and the pump geometry carefully designed to maximise efficiency. On the other hand, they are definitely more attractive than glasses for power upscaling, owing to their superior thermal and mechanical properties.

7. Acknowledgement

We acknowledge the contribution of Bright Solutions, Srl, for supporting and discussion. This research received funding from the European Community's Seventh Framework Programme FP7/2007-2011 under grant agreement n◦ 224042.

8. References

Agnesi, A.; Reali, G. C.; Kubecek, V.; Kumazaki, S.; Takagi, Y. & Yoshihara, K. (1993). β-barium borate and lithium triborate picosecond parametric oscillators pumped by a frequency-tripled passive negative-feedback mode-locked Nd:YAG laser. *Journal of the Optical Society of America B*, Vol. 10, No. 11, (November 1993) pp. 2211-2217, ISSN: 0740-3224

Agnesi, A.; Pirzio, F.; Tomaselli, A.; Reali, G. & Braggio, C. (2005). Multi-GHz tunable-repetition-rate mode-locked Nd:$GdVO_4$ laser. *Optics Express*, Vol. 13, No. 14, (July 2005) pp. 5302-5307, ISSN: 1094-4087

Agnesi, A.; Carrà, L.; Pirzio, F.; Reali, G.; Tomaselli, A.; Scarpa, D. & Vacchi, C. (2006a). Amplification of a low-power picosecond Nd:YVO_4 laser by a diode-laser side-pumped grazing-incidence slab amplifier. *IEEE Journal of Quantum Electronics*, Vol. 42, No. 8, (August 2006) pp. 772-776, ISSN: 0018-9197

Agnesi, A.; Carrà, L.; Pirzio, F.; Scarpa, D.; Tomaselli, A.; Reali, G.; Vacchi, C. & Braggio, C. (2006b). High-gain diode-pumped amplifier for generation of microjoule-level picosecond pulses. *Optics Express*, Vol. 14, No. 20, (October 2006) pp. 9244-9249, ISSN: 1094-4087

Agnesi, A.; Carrà, L.; Dallocchio, P.; Pirzio, F.; Reali, G.; Tomaselli, A.; Scarpa, D. & Vacchi, C. (2008a). 210-μJ picosecond pulses from a quasi-cw Nd:YVO_4 grazing-incidence two-stage slab amplifier package. *IEEE Journal of Quantum Electronics*, Vol. 44, No. 10, (October 2008) pp. 952-957, ISSN: 0018-9197

Agnesi, A.; Braggio, C.; Carrà, L.; Pirzio, F.; Lodo, S.; Messineo, G.; Scarpa, D.; Tomaselli, A.; Reali, G. & Vacchi, C. (2008b). Laser system generating 250-mJ bunches of 5-GHz repetition rate, 12-ps pulses. *Optics Express*, Vol. 16, No. 20, (September 2008) pp. 15811-15815, ISSN: 1094-4087

Bermudez, J. C. G.; Pinto-Robledo, V. J.; Kir'yanov, A.V. & Damzen M. J. (2002). The thermo-lensing effect in a grazing incidence, diode-side-pumped Nd:YVO_4 laser. *Optics Communications*, Vol. 210, No. 1-2, (September 2002) pp. 75-82, ISSN: 0030-4018

Bernard, J. E. & Alcock, A. J. (1993). High-efficiency diode-pumped Nd:YVO_4 slab laser. *Optics Letters*, Vol. 18, No. 12, (June 1993) pp. 968-970, ISSN: 0146-9592

Breitling, D.; Ruf, A. & Dausinger, F. (2004). Fundamental aspects in machining of metals with short and ultrashort laser pulses, Proceedings of SPIE Vol. 5339 Photon processing in microelectronics and photonics III, pp. 49-63, ISBN 9780819452474, San Jose CA (USA), January 2004, SPIE, Bellingham WA (USA)

Burns, D.; Hetterich, M.; Ferguson, A. I.; Bente, E.; Dawson, M. D.; Davies, J. I. & Bland, S. W. (2000). High-average power (>20-W) Nd:YVO_4 lasers mode locked by strain-compensated saturable Bragg reflectors. *Journal of the Optical Society of America B*, Vol. 17, No. 6, (June 2000) pp. 919-926, ISSN: 0740-3224

Butterworth, S. D.; Clarkson, W. A.; Moore, N.; Friel, G. J. & Hanna, D. C. (1996). High-power quasi-cw laser pulses via high-gain diode-pumped bulk amplifiers. *Optics Communications*, Vol. 131, No. 1-3, (October 1996) pp. 84-88, ISSN: 0030-4018

Damzen, M. J.; Trew, M.; Rosas, E. & Crofts G.J. (2001). Continuous-wave Nd:YVO_4 grazing-incidence laser with 22.5 W output power and 64% conversion efficiency. *Optics Communications*, Vol. 196, No. 1-6, (September 2001) pp. 237-241, ISSN: 0030-4018

Dausinger, F.; Hügel, H. & Konov, V. (2003). Micro-machining with ultrashort laser pulses: from basic understanding to technical applications, Proceedings of SPIE Vol. 5147 ALT'02 International Conference on Advanced Laser Technologies, pp. 106-115, ISBN 9780819450173, Adelboden (Switzerland), November 2003, SPIE, Bellingham WA (USA)

Edwards, G. S.; Hutson, M. S.; Hauger, S.; Kozub, J. A.; Shen, J.-H.; Shieh, C.; Topadze, K. & Joos, K. (2002). Comparison of OPO and Mark-III FEL for tissue ablation at 6.45 μm, Proceedings of SPIE Vol. 4633 Commercial and biomedical applications of ultrafast and free-electron lasers, pp. 194-200, ISBN 9780819443724, San Jose CA (USA), April 2002, SPIE, Bellingham WA (USA)

Farrell, D. J. & Damzen, M. J. (2007). High power scaling of a passively modelocked oscillator in a bounce geometry. *Optics Express*, Vol. 15, No. 8, (April 2007) pp. 4781-4786, ISSN: 1094-4087

Fermann, M. E. & Hartl, I. (2009). Ultrafast fiber laser technology. *IEEE Journal of Selected Topics in Quantum Electronics*, Vol. 15, No. 1, (January 2009) pp. 191-206, ISSN: 1077-260X

Flood, C. J.; Walker, D. R. & Van Driel, H. M. (1995). Effect of spatial hole burning in a mode-locked diode end-pumped Nd:YAG laser. *Optics Letters*, Vol. 20, No. 1, (January 1995) pp. 58-60, ISSN: 0146-9592

Frantz L. M. & Nodvik, J. S. (1963). Theory of pulse propagation in a laser amplifier. *Journal of Applied Physics*, Vol. 34, No. 8, (August 1963) pp. 2346-2349, ISSN: 0021-8979

Gerhard, C.; Druon, F.; Blandin, P.; Hanna, M.; Balembois, F.; Georges, P. & Falcoz, F. (2008). Efficient versatile-repetition rate picosecond source for material processing applications. *Applied Optics*, Vol. 47, No. 7, (March 2008) pp. 967-974, ISSN: 0003-6935

Keller U. (2003). Recent developments in compact ultrafast lasers. *Nature*, Vol. 424, (August 2003) pp. 831-838, ISSN: 0028-0836

Killi, A.; Dörring, J.; Morgner, U.; Lederer, M. J.; Frei, J. & Kopf, D. (2005). High speed electro-optical cavity dumping of mode-locked laser oscillators. *Optics Express*, Vol. 13, No. 6, (March 2005) pp. 1916-1922, ISSN: 1094-4087

Kleinbauer, J.; Knappe, R. & Wallenstein, R. (2005). 13-W picosecond Nd:$GdVO_4$ regenerative amplifier with 200-kHz repetition rate. *Applied Physics B*, Vol. 81, No. 2-3, (July 2005) pp. 163-166, ISSN: 0946-2171

Koechner, W. (2006). *Solid-State Laser Engineering*, Springer, ISBN 9780387290942, Berlin

Le Blanc, C.; Curley, P. & Salin, F. (1996). Gain-narrowing and gain-shifting of ultra-short pulses in Ti:sapphire amplifiers. *Optics Communications*, Vo. 131, No. 4-6, (November 1996) pp. 391-398, ISSN: 0030-4018

Mani, A. A.; Dreesel, L.; Hollander, P.; Humbert, C.; Caudano, Y.; Thiry, P. A. & Peremans, A. (2001). Pumping picosecond optical parametric oscillators by a pulsed Nd:YAG laser mode locked using a nonlinear mirror. *Applied Physics Letters*, Vol. 79, No. 13, (September 2001) pp. 1945-1947, ISSN: 0003-6951

McCarthy, M. J. & Hanna, D. C. (1993). All-solid-state synchronously pumped optical parametric oscillator. *Journal of the Optical Society of America B*, Vol. 10, No. 11, (November 1993) pp. 2180-2189, ISSN: 0740-3224

McDonagh, L.; Wallenstein, R. & Nebel, A. (2007). 111 W, 110 MHz repetition-rate, passively mode-locked TEM_{00} Nd:YVO_4 master oscillator power amplifier pumped at 888 nm. *Optics Letters*, Vol. 32, No. 10, (May 2007) pp. 1259-1261, ISSN: 0146-9592

Minassian, A.; Thompson, A.; Smith, G. & Damzen, M. J. (2005). High-power scaling (>100 W) of a diode-pumped TEM_{00} Nd:$GdVO_4$ laser system. *IEEE Journal of Selected Topics in Quantum Electronics*, Vol. 11, No. 3, (May/June 2005) pp. 621-625, ISSN: 1077-260X

Nawata, K.; Ojima, Y.; Okida, M.; Ogawa, T.& Omatsu T. (2006). Power scaling of a picosecond Nd:YVO_4 master-oscillator power-amplifier with a phase-conjugate mirror. *Optics Express*, Vol. 14, No. 22, (October 2006) pp. 10657-10662, ISSN: 1094-4087

Nawata, K.; Okida, M.; Furuki, K. & Omatsu, T. (2007). MW ps pulse generation at sub-MHz repetition rate from a phase-conjugate Nd:YVO_4 bounce amplifier. *Optics Express*, Vol. 15, No. 15, (July 2007) pp. 9123-9128, ISSN: 1094-4087

Neuhaus, J.; Kleinbauer, J.; Killi, A.; Weiler, S.; Sutter, D. & Dekorsy, T. (2008). Passively mode-locked Yb:YAG thin-disk laser with pulse energies exceeding 13 μJ by use of an active multipass geometry. *Optics Letters*, Vol. 33, No. 7, (April 2008) pp. 726-728, ISSN: 0146-9592

Ojima, Y.; Nawata, K. & Omatsu T. (2005). Over 10-W picosecond diffraction-limited output from a Nd:YVO_4 slab amplifier with a phase conjugate mirror. *Optics Express*, Vol. 13, No. 22, (October 2005) pp. 8993-8998,, ISSN: 1094-4087

Okhotnikov, O. G.; Gomes, L. A.; Xiang, N.; Jouhti, T.; Chin, A. K.; Singh, R. & Grudinin A. B.(2003). 980-nm Picosecond Fiber Laser. *IEEE Photonics Technology Letters*, Vol. 15, No. 11, (November 2003) pp. 1519-1521, ISSN: 1041-1135

Porta, J.; Grudinin, A. B.; Chen, Z. J.; Minelly, J. D. & Traynor, N. J. (1998). Environmentally stable picosecond ytterbium fiber laser with a broad tuning range. *Optics Letters*, Vol. 23, No. 8, (April 1998) pp. 615-617, ISSN: 0146-9592

Rufling, B.; Nebel, A. & Wallenstein, R. (2001). High-power picosecond LiB_3O_5 optical parametric oscillators tunable in the blue spectral range. *Applied Physics B*, Vol. 72, No. 2, (January 2001) pp. 137-149, ISSN: 0946-2171

Siebold, M.; Hornung, M.; Hein, J.; Paunescu, G.; Sauerbrey, R.; Bergmann, T. & Hollemann, G. (2004). A high-average power diode-pumped Nd:YVO_4 regenerative laser amplifier for picosecond-pulses. *Applied Physics B*, Vol. 78, No. 3-4, (February 2004) pp. 287-290, ISSN: 0946-2171

Snell, K. J.; Lee D.; Wall, K. F. & Moulton, P. F. (2000). Diode-pumped, high-power cw and modelocked Nd:YLF lasers, OSA Trends in Optics and Photonics Vol. 34, pp. 55-59, ISBN 1557526281, Davos (Switzerland), February 2000, Optical Society of America, Washington, D.C.

Sun, Z.; Ghotbi, M. & Ebrahimzadeh, M. (2007). Widely tunable picosecond optical parametric generation and amplification in BiB_3O_6. *Optics Express*, Vol. 15, No. 7, (April 2007) pp. 4139-4147, ISSN: 1094-4087

Walker, D. R.; Flood, C. J.; van Driel, H. M.; Greiner, U. J. & Klingerberg, H. H. (1994). High power diode-pumped Nd:YAG regenerative amplifier for picosecond pulses. *Applied Physics Letters*, Vol. 65, No. 16, (October 1994) pp. 1992-1994

Will, I.; Koss, G. & Templin, I. (2005). The upgraded photocatode laser of the TESLA Test Facility. *Nuclear Instruments and Methods in Physics Research. Section A*, Vol. 541, No. 3, (April 2005) 467-477, ISSN: 0168-9002

Zayhowski, J. J. & Harrison, J. (1997). Miniature solid-state lasers, in: *Handbook of Photonics*, Gupta, M. C., (Ed.), pp. 326-392, CRC Press, ISBN 0849389097, Boca Raton FL (USA)